Structural Engineering and Mechanics, *Vol. 54, No. 5 (2015) 855-875*
DOI: http://dx.doi.org/10.12989/sem.2015.54.5.855

Nonlinear large deflection buckling analysis of compression rod with different moduli

Wenjuan Yao[*1], Jianwei Ma[1a], Jinling Gao[1b] and Yuanzhong Qiu[2a]

[1]*Department of Civil Engineering, Shanghai University, Shanghai 200072, China*
[2]*SEGOC, West Rd., Houston TX 77041, USA*

(Received April 19, 2014, Revised November 9, 2014, Accepted November 11, 2014)

Abstract. Many novel materials exhibit a property of different elastic moduli in tension and compression. One such material is graphene, a wonder material, which has the highest strength yet measured. Investigations on buckling problems for structures with different moduli are scarce. To address this new problem, firstly, the nondimensional expression of the relation between offset of neutral axis and deflection curve is derived based on the phased integration method, and then using the energy method, load-deflection relation of the rod is determined; Secondly, based on the improved constitutive model for different moduli, large deformation finite element formulations are developed and combined with the arc-length method, finite element iterative program for rods with different moduli is established to obtain buckling critical loads; Thirdly, material mechanical properties tests of graphite, which is the raw material of graphene, are performed to measure the tensile and compressive elastic moduli, moreover, buckling tests are also conducted to investigate the buckling behavior of this kind of graphite rod. By comparing the calculation results of the energy method and finite element method with those of laboratory tests, the analytical model and finite element numerical model are demonstrated to be accurate and reliable. The results show that it may lead to unsafe results if the classic theory was still adopted to determine the buckling loads of those rods composed of a material having different moduli. The proposed models could provide a novel approach for further investigation of non-linear mechanical behavior for other structures with different moduli.

Keywords: different moduli; buckling compression rod; analytical method; numerical method; laboratory tests

1. Introduction

A new research has indicated that graphene, the strongest material (Geim 2009) yet known, has been verified as a material with different moduli. That is, the compressive elastic modulus is larger than the tensile elastic modulus (Tsoukleri *et al*. 2009). For many civil engineering materials, such as concrete (Zhou *et al*. 2005), metal (Gilbert 1961), foam plastic (Rizzi 2000), rubber (Patel 1976), biomaterial (Barak *et al*. 2009), and rock (Haimson and Tharp 1974), it has been

∗Corresponding author, Professor, E-mail: wjyao@shu.edu.cn
[a]Ph.D. Student
[b]Master Student

Copyright © 2015 Techno-Press, Ltd.
http://www.techno-press.org/?journal=sem&subpage=8 ISSN: 1225-4568 (Print), 1598-6217 (Online)

experimentally demonstrated that the elastic properties in extension differ from those in contraction. Particularly, for the composite materials that are made of carbon fibers, the ratio of their different modulus can be as high as five (Kratsh *et al*. 1972). Therefore, the difference between materials with different moduli and those with the same modulus, which determines the mechanical behavior of structures, can not be neglected.

Generally, there are two basic models for representing materials with different moduli. The elastic parameters of these two models are selected based on two different criterions separately. One is proposed by Bert (1977), Jones (1977), namely, “longitudinal fiber direction criterion”, which is applicable for the study on structures consisting of stratified composite. The other is presented by Ambartsumyan (1986), that is, “principal stress sign criterion”, which is adequate for the investigation of structures that are composed of natural materials and polymeric materials. To extensively and effectively be applied in engineering,Ambartsumyan’s model is improved by Vijayakumar and Ashoka (1990), Ye *et al*. (2001), who respectively put forward two constitutive models that are bilinear biaxial principal stress model and principal strain model.

Early on, researchers tended to rely on finite element method to investigate structures with different moduli. Zhang and Wang (1989) firstly proposed finite element iterative technique to solve problems with different moduli. Due to unstable iteration and slow convergency of this method, Liu and Zhang (2000), He *et al*. (2009) respectively adopted the shear modulus method to increase the rate of iteration and convergence. Likewise, Yang *et al*. (1992, 1999, 2006, 2008) exploited initial stress and smoothing techniques to simplify the process of finite element iteration, thus leading to a higher computing efficiency. Using the finite element method, most studies on structures with different moduli have focused mainly on strength analysis. Zhang and Wang (1989) analyzed the stress and deformation of rigid frame with different moduli; Gong *et al*. (1994) analyzed the problem of round hole expansion; Patel (2004) investigated the thermo-flexural analysis of thick laminated composites; Raffaele and Fabrizio (2001) carried out a damage evolution analysis of laminated composites under cyclic loading; and Tseng and Jiang (1998) performed a stress analysis of laminates.

In view of the peculiar nonlinear (bilinear or piecewise linear) characteristics of different moduli problems, Yao and Ye (2004a, b) resorted to the flowing coordinate system and phased integration method to present analytical solutions for the neutral axis, stress, strain and displacement of a beam-column, and of a beam under lateral load. Yao *et al*. (2006a, b) also developed the iterative programme for calculating nonlinear internal forces of statically indeterminate structures, and of combined members with different moduli under complex stress state. He (2007) obtained the approximate elasticity solution of a bimodular beam and a bimodular bending-compression column by employing the equivalent section method. Based on the equivalent modulus of elasticity of analytical solution for bending-compression column (Yao and Ye, 2004b), Qu (2009) derived the analytical solution for the deflection of geocell with different tension and compression modulus. Leal (2009) derived the compressive strength equation of high performance fibers with different moduli and analyzed the effects of bimodularity on the compressive strength.

The previous studies on the structures with different moduli mainly focused on the strength analysis, among which most analysis only concerned material nonlinearity characteristic and the others also involved geometric nonlinearity behavior of the composite plates (Bruno *et al*. 1994) and sandwich beams (Lan *et al*. 2003) with different moduli. Additionally, the constitutive models of these materials with different moduli were both based on Bert’s and Jone’s model (1977a, b).

Investigations on stability of structures with different moduli are scant and more complex versus strength problems. For Ambartsumyan's principal stress criterion, because the tension-compression dividing layer (neutral axis) depends not only on the material property itself but also on the principal stress state of each point, the determination of the neutral axis is a nonlinear problem relevant to both the elastic modulus and deflection equation. Regarding this problem, Rigbi (1973) presented a strain energy criterion to determine the buckling state of columns with different moduli. Based on this criterion, Rigbi and Shlomo (1978) obtained approximate buckling critical loads by assuming the relation of external load and deflection. However, this method was not tested and verified and also too complex to be of practical use. Bert and Ko (1985) used the finite difference method to analyze the buckling behavior of cantilever column with different moduli. Nonetheless, these investigations were only limited to small deformation assumption.

The small deformation theory assumes that the curvature of neutral layer approximately equals to that of midline for the cross section. In addition, the curvature approximates as second derivative of deflection function in order to simplify the derivation process. Actually, only if the elastic moduli in tension and compression are numerically equal can this assumption be satisfied. Furthermore, under the small deformation theory, in the buckling critical state, the neutral axis offset (only the offset in the position of the maximum deflection be reckoned in) assumes a constant along the length of rod. However, for the rod with different moduli in the buckling critical state, the neutral axis offset actually changes along the length of rod. Therefore, to obtain a more accurate solution should be based on large deformation theory.

In view of this, the buckling problem of rod with different moduli is a complicated double nonlinear problem. Graphene is a new material with a different moduli. It is well known for its high strength. However, the dominant failure of structures composed of this high strength material is often attributed to buckling problems. With the above considerations, buckling analysis of rod with different moduli is performed and the rest of the paper isorganized as follows. In Section 2, we present basic assumptions and structural model that is to be analyzed. In Section 3, according to static for balance condition and Saint Venant principle, the dimensionless relation formula of neutral axis offset and deflection curve is deduced. In Section 4, using the energy method, we derive the relation formula of externalload and deflection of rod. In Section 5, based on the improved constitutive model fordifferent moduli, large deformation finite element formulations are developed and combinedwith the arc-length method, finite element iterative program for rods with different moduli is established to obtain buckling critical loads. In Section 6, in order to verify the analytical model and the numerical model presented in this paper, material mechanical properties tests and buckling tests are performed. In Section 7, the effects of different moduli on the stability of rod are investigated. In Section 8, we conclude the paper.

2. Basic assumption and structural model

Subject to tensile or compressive stress with the same absolute value, a material will produce a corresponding tensile or compressive strain with different absolute values. This suggests that materials have a different tensile modulus E_t and compressive modulus E_c. The constitutive bilinear model (Jones 1977), as shown in Fig. 1, in which the slope of the straight line is discontinuous in the origin, is used in this paper.

Assume the investigated object to be continuous, homogeneous, and isotropic solid. Dueto the difference in the sign of principal stress, the material demonstrates different elastic properties and satisfies the general law of continual medium mechanics (Ambartsumyan 1986). Moreover, the

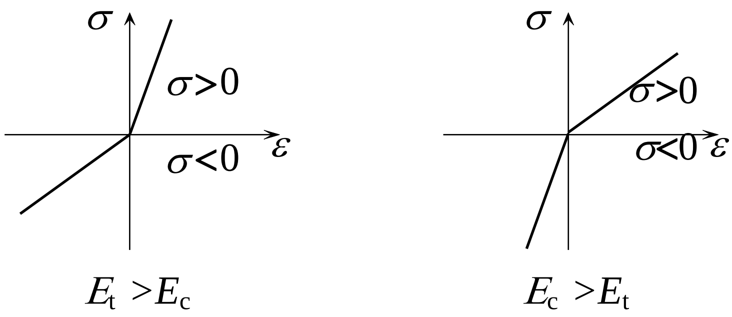

Fig. 1 Constitutive relationship of materials with different moduli (bilinear model)

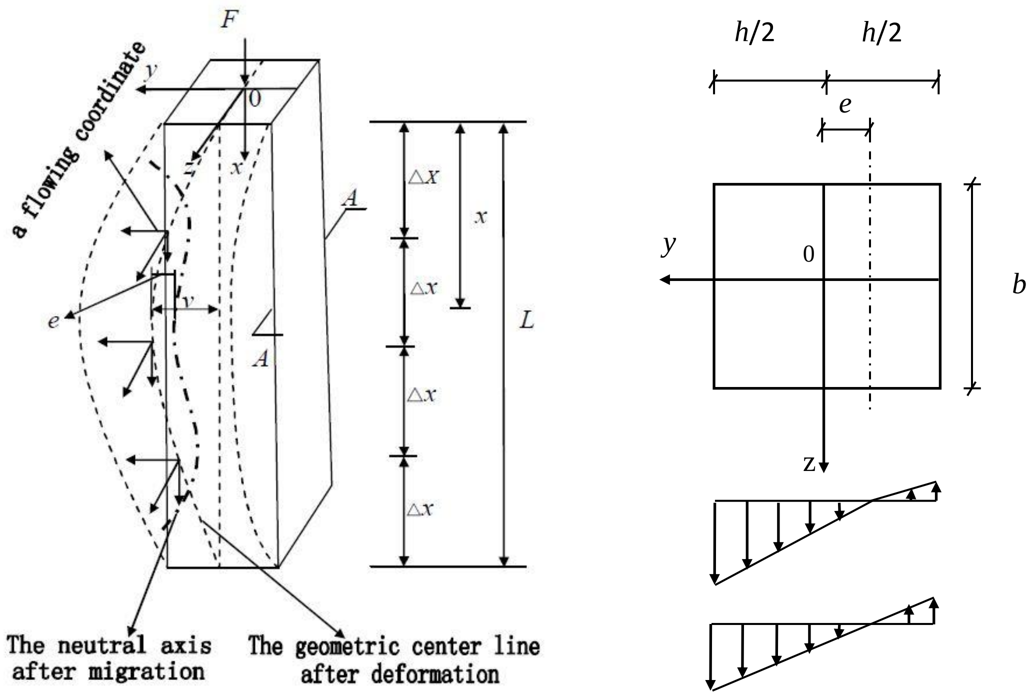

(a) (b)

Fig. 2 (a) Buckling of pin-ended slender rod, and (b) cross-section *A*-*A*

material only produces elastic deformation in a random stress state, andtherefore, basic equations are identical to that of the same modulus elastic theory and the difference is only reflected in thephysical equation.

Consider a uniform elastic slender rod of length L, geometric size $b \times h$, a rectangular cross-section, neglecting the body weight, and it is subjected to an axial force F applied in the center at one end of the rod (see Fig. 2(a)). Assumes the symbol e (hereinafter referred to as the offset) denotes the distance between the neutral axis and the geometrical center line. When the neutral axis moves to the tensile zone, the sign of e is positive, and vice versa. The stress and strain distribution of any *A*-*A* cross section is shown in Fig. 2(b). In the buckling critical state, the neutral axis of the *y-o-z* plane will vary along the *x*-axis, that is, the offset $e=f(x)$. Therefore, a flowing coordinate system is adopted. After each increment Δx is added along the *x*-axis, the coordinate axis will move and the coordinate axis of each section in the *y-o-z* plane will pass through the neutral axis (Fig. 2(a)).

3. Derivation of dimensionless relation between neutral axis offset and deflection

The rod is assumed to bend about a certain principal axis of inertia without axial deformation and plane cross section assumption is also made. The normal strain of a random point in *x*-direction can be expressed as

$$\varepsilon_x = \frac{y-e}{\rho} \qquad \text{in which} \quad \frac{1}{\rho} = \frac{d^2\bar{v}}{dx^2} \Bigg/ \left[1+\left(\frac{d\bar{v}}{dx}\right)^2\right]^{3/2} \tag{1}$$

where $\bar{v}=e+v$, e is the neutral axis offset, v and $\bar{v}$ are deflection of rod in y direction, relative displacement between geometric center line before deformation and neutral axis after migration. When the axial load begins to increase from zero, prior to buckling there is a compressive state in the whole cross section of rod. With the load increasing, bending deformation has taken place in the rod, in the cross section of which tensile stress emerges.Then deformation develops rapidly and the cross-section has been divided into distinct tensile zone and compressive zone, as shown in Fig. 3.

According to the bilinear constitutive relationship based on the elastic theory of different moduli, the normal stress from different regions can be written as follows

$$\sigma_{\mathrm{t}} = E_{\mathrm{t}}\frac{y-e}{\rho} \qquad \sigma_{\mathrm{c}} = E_{\mathrm{c}}\frac{y-e}{\rho} \tag{2}$$

Take the *A*-*A* cross-section and the above from the rod and invokes the internal force equilibrium condition gives

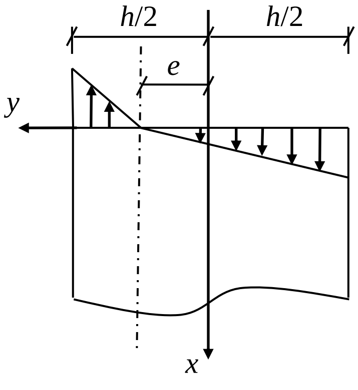

Fig. 3 Stress distribution of the cross section

$$F=\int_{-h/2}^{e}E_{\mathrm{c}}\frac{b(y-e)}{\rho}dy+\int_{e}^{h/2}E_{\mathrm{t}}\frac{b(y-e)}{\rho}dy=\frac{bh^2}{2\rho}\left[-E_{\mathrm{c}}(1/2+\zeta)^2+E_{\mathrm{t}}(1/2-\zeta)^2\right] \tag{3}$$

where $\zeta=e/h$. According to the Saint-Venant principle, the bending moment of any cross-section A-A is given by

$$M=\int_{e}^{h/2}E_{\mathrm{t}}\frac{b(y-e)^2}{\rho}dy+\int_{-h/2}^{e}E_{\mathrm{c}}\frac{b(y-e)^2}{\rho}dy=\frac{bh^3}{3\rho}\left[E_{\mathrm{t}}(1/2-\zeta)^3+E_{\mathrm{c}}(1/2+\zeta)^3\right] \tag{4}$$

Invoking the equilibrium condition, we can get

$$F\bar{v}=M \tag{5}$$

Substituting Eq. (3) and Eq. (4) into Eq. (5) gives

$$\begin{aligned}&5(1-m)\zeta^3+\left[3\eta(1-m)-6(m+1)\right]\zeta^2+3\left[\frac{3}{4}(1-m)-\eta(m+1)\right]\zeta\\&+\frac{1}{4}\left[3\eta(1-m)-(m+1)\right]=0\end{aligned} \tag{6}$$

where $\eta=\bar{v}/h$, $m=E_c/E_t$. In Eq. (6), there exists a complicated nonlinear relationship among ζ, m, and η. In other words, the offset changes with both the ratio of different moduli and deflection function. The definite expression of ζ can be obtained via Mathematic software.Because of limitation of length, no calculation results of ζ listed here. The Eq. (6) also can be expressed as

$$\begin{aligned}&\left[3(1-m)\zeta^2-3(m+1)\zeta+\frac{3}{4}(1-m)\right]\eta+5(1-m)\zeta^3-6(m+1)\zeta^2\\&+\frac{9}{4}(1-m)\zeta-\frac{1}{4}(m+1)=0\end{aligned} \tag{7}$$

According to Eq. (7), when m is a given value, ζ will changes with increasing η . However, the neutral axis will move with some limitation. Therefore, when $\eta\to+\infty$, the coefficient of η in Eq. (7) should be zero so as to make ζ be bounded. So it leads to

$$3(1-m)\zeta^2-3(m+1)\zeta+\frac{3}{4}(1-m)=0 \tag{8}$$

Solving Eq. (8), the ultimate stable value of dimensionless offset can be obtained

$$\zeta_1=\frac{-(m+1)+2\sqrt{m}}{2(m-1)};\ \zeta_2=\frac{-(m+1)-2\sqrt{m}}{2(m-1)}\quad\text{(abandoned)} \tag{9}$$

Once the dimensionless relation expression between ζ and η is determined, using the energy method (hereinafter referred to as EM for short), we can move forward to calculate relation formula of external load and deflection of rod and finally obtain the buckling critical load.

4. The establishment of calculation formula with EM

It should be noted that the offset varies along the length of rod. If the neutral axis of all cross section presumes to be located outside the boundary of cross section, the strain energy of rod can be written as

$$U=\frac{1}{2}\int_0^{L-d}\int_{-h/2}^{h/2}\frac{bE_{\mathrm{c}}(y-e)^2}{\rho^2}dydx=\frac{bE_{\mathrm{c}}}{2}\int_0^{L-d}\frac{1}{\rho^2}\frac{1}{3}\left[(e+h/2)^3-(e-h/2)^3\right]dx \tag{10}$$

where d is axial displacement of rod end. According to $\bar{v}=e+v$, $\zeta=e/h$, $\eta=v/h$, Eq. (1), Eq. (3) and $\bar{x}=x/(L-d)$, Eq. (10) can be smplified as

$$U=\frac{2F^2(L-d)}{3bhE_c}\int_0^1\frac{\left[(1/2+\zeta)^3-(\zeta-1/2)^3\right]}{\left[(\zeta+1/2)^2-(1/2-\zeta)^2\right]^2}d\bar{x} \tag{11}$$

Simplifying Eq. (11) can lead to

$$U=\frac{2F^2(L-d)}{bhE_c}\int_0^1(3\eta^2+\frac{1}{4})d\bar{x} \tag{12}$$

Similarly, if the neutral axis of all cross sections presumes to be located inside the boundary of cross-section, the strain energy of rod can be shown as

$$\begin{aligned}U&=\frac{b}{2}\int_0^{L-d}\left[\int_e^{h/2}E_{\mathrm{t}}\frac{(y-e)^2}{\rho^2}dy+\int_{-h/2}^{e}E_{\mathrm{c}}\frac{(y-e)^2}{\rho^2}dy\right]dx\\&=\frac{bE_{\mathrm{t}}}{6}\int_0^{L-d}\frac{1}{\rho^2}\left[(h/2-e)^3+m(h/2+e)^3\right]dx\end{aligned} \tag{13}$$

Simplifying Eq. (13) can give

$$U=\frac{3F^2(L-d)}{2bhE_t}\int_0^1\frac{(\eta+\zeta)^2}{\left[(1/2-\zeta)^3+m(1/2+\zeta)^3\right]}d\bar{x} \tag{14}$$

An external force F produces the work

$$W=F\cdot d \tag{15}$$

As the external work increases, the strain energy grows equally. Based on energy theory, it is found that $\Delta U-\Delta W=0$. For both ends simply supported rod with different moduli, within the range of an assumed distance a from both ends of rod to specified positions along the length of rod, the neutral axis is located outside cross section, and vice versa. Thus, in different regions, the strain energy should be established based on Eq. (12) and Eq. (14) respectively. Then we get

$$F\cdot d=\frac{3F^2(L-d)}{2bhE_t}\int_a^{1-a}\frac{(\eta+\zeta)^2}{[(1/2-\zeta)^3+m(1/2+\zeta)^3]}d\bar{x}+\frac{2F^2(L-d)}{bhE_c}\left[\int_0^a(3\eta^2+\frac{1}{4})d\bar{x}+\int_{1-a}^1(3\eta^2+\frac{1}{4})d\bar{x})\right] \tag{16}$$

Simplifying Eq. (16) gives

$$\frac{F(L-d)}{dbhE_t}=\frac{1}{\left[3\int_a^{1-a}\frac{(\eta+\zeta)^2}{[(1/2-\zeta)^3+m(1/2+\zeta)^3]}d\bar{x}+\frac{12\times 2}{m}\left(\int_{1-a}^{1}\eta^2 d\bar{x}+\frac{1}{2}a\right)\right]} \tag{17}$$

where the relation between the external load and deflection of rod is reflected. In order to deermine the nonlinear mechanical behavior of the buckling rod, some parameters, including axial deformation d, a, the form of deflection curve, should be ascertained. In addition, the intricate integral operation in Eq. (18) can be solved by employing Romberg Integral Method.

Take no account of axial strain and we get

$$L=\int_0^{L-d}\sqrt{1+\left(\frac{dv}{dx}\right)^2}dx \tag{18}$$

Expanding Eq. (18) using Taylor series and simplifying it

$$\frac{(L-d)^3}{L^3}-\frac{(L-d)^2}{L^2}+\frac{h^2}{L^2}\frac{1}{2}\int_0^1\left(\frac{d\eta}{dx}\right)^2 dx\left(\frac{L-d}{L}\right)=0 \tag{19}$$

From Eq. (19), we learn that the determination of d should rely on a known η. Herein, the deflection function of both ends simply supported rod assumed reasonably to be

$$\eta=\frac{v_m}{h}\sin\left(\frac{\pi x}{L}\right) \tag{20}$$

where v_m is the mximum deflection of rod. Substituting Eq. (20) into Eq. (19) can get d. When the neutral axis is located on the geometric boundary of rod, ζ=0.5. Then substitute ζ and Eq. (20) into Eq. (7), for different ratio of different moduli, the parameter a can be solved.

5. The establishment of finite element method

In this section, the finite element method (FEM) is adopted to solve the nonlinear buckling problem of rod with different moduli. Owing to the aforementioned assumption that the rod only bends about one principal axis of inertia and no twist and no warpage occur, large deformation finite element formulation of rod with different moduli is developed in two-dimension space in the following part.

5.1 The modified constitutive model based on elastic theory with different moduli

Based on the principal strain criterion (Ye *et al*. 2001), the constitutive matrix can be written as:

$$\boldsymbol{D}_I=\frac{E_tE_c}{1-\mu^2}\begin{pmatrix}\frac{1}{E_c} & \frac{\mu}{E_c}\\ \frac{\mu}{E_t} & \frac{1}{E_t}\end{pmatrix}\quad \text{or}\quad \boldsymbol{D}_I=\frac{E_tE_c}{1-\mu^2}\begin{pmatrix}\frac{1}{E_t} & \frac{\mu}{E_t}\\ \frac{\mu}{E_c} & \frac{1}{Ec}\end{pmatrix} \tag{21}$$

where $\mu = \dfrac{\mu_t + \mu_c}{2}$, μ_t and μ_c are elastic tensile Poisson ratio and elastic compressive Poisson ratio respectively, $\mathbf{D}_I$ is elastic matrix regarding principal stress and principal strain. To explore the influence of variation of different moduli on calculation results, for convenience, the elastic matrix is nondimensionalized and modified (Ye *et al*. 2001), thus the constitutive relationship can be written as

$$\boldsymbol{\sigma} = \overline{\boldsymbol{L}}^T \overline{\boldsymbol{\sigma}}_I = \overline{\boldsymbol{L}}^T \overline{\overline{\mathbf{D}}}_I \overline{\boldsymbol{\varepsilon}}_I = \overline{\boldsymbol{L}}^T \overline{\overline{\mathbf{D}}}_I \overline{\boldsymbol{L}} \boldsymbol{\varepsilon} = \overline{\boldsymbol{D}} \boldsymbol{\varepsilon} \tag{22}$$

where $\overline{\boldsymbol{D}}$ is equivalent modified elastic matrix regarding stress and strain and $\overline{\boldsymbol{L}}$ is coordinate transfer matrix, written as

$$\overline{\boldsymbol{L}} = \begin{pmatrix} {l_1}^2 & {m_1}^2 & l_1 m_1 \\ {l_2}^2 & {m_2}^2 & l_2 m_2 \\ 2 l_1 l_2 & 2 m_1 m_2 & l_1 m_2 + l_2 m_1 \end{pmatrix} \tag{23}$$

5.2 Plane large deformation finite element formulation with different moduli

The large deformation nonlinear strain-displacement relation formula can be expressed as

$$\begin{cases} \varepsilon_x = \dfrac{\partial u}{\partial x} + \dfrac{1}{2}\left[\left(\dfrac{\partial u}{\partial x}\right)^2 + \left(\dfrac{\partial v}{\partial x}\right)^2\right], \quad \varepsilon_y = \dfrac{\partial v}{\partial y} + \dfrac{1}{2}\left[\left(\dfrac{\partial u}{\partial y}\right)^2 + \left(\dfrac{\partial v}{\partial y}\right)^2\right] \\ \gamma_{xy} = \dfrac{\partial v}{\partial x} + \dfrac{\partial u}{\partial y} + \dfrac{\partial u}{\partial x}\dfrac{\partial u}{\partial y} + \dfrac{\partial v}{\partial x}\dfrac{\partial v}{\partial y} \end{cases} \tag{24}$$

where u and v are components of nodal displacement $\boldsymbol{u}$ in direction x and y respectively, ε_x, ε_y and γ_{xy} are components of strain $\boldsymbol{\varepsilon}$. $\boldsymbol{\varepsilon}$, which can be divided into linear strain $\boldsymbol{\varepsilon}_L$ and nonlinear strain $\boldsymbol{\varepsilon}_{NL}$, can be written as

$$\boldsymbol{\varepsilon} = \boldsymbol{\varepsilon}_L + \boldsymbol{\varepsilon}_{NL} = \boldsymbol{B}_L \boldsymbol{u}^e + \overline{\boldsymbol{B}}_{NL} \boldsymbol{u}^e = \left(\boldsymbol{B}_L + \overline{\boldsymbol{B}}_{NL}\right)\boldsymbol{u}^e = \overline{\boldsymbol{B}} \boldsymbol{u}^e \tag{25}$$

where $\boldsymbol{B}_L$ and $\overline{\boldsymbol{B}}_{NL}$ are linear and nonlinear transfer matrix of strain and displacement, $\boldsymbol{u}^e$ is element nodal displacement. Variation of Eq. (25) can be shown that

$$\delta\boldsymbol{\varepsilon} = \left(\boldsymbol{B}_L + 2\overline{\boldsymbol{B}}_{NL}\right)\delta\boldsymbol{u}^e = \boldsymbol{B}\delta\boldsymbol{u}^e \tag{26}$$

Substituting Eq. (26) into virtual work equation

$$\int_{\Omega_e} (\delta\boldsymbol{\varepsilon})^T \boldsymbol{\sigma} \mathrm{d}\Omega = \delta\boldsymbol{u}^{e^T} \int_{\Omega_e} \boldsymbol{B}^T \boldsymbol{\sigma} \mathrm{d}\Omega = \delta\boldsymbol{u}^{e^T} \boldsymbol{P}^e \tag{27}$$

and due to randomly selectivity of $\delta\boldsymbol{d}^e$, we get

$$R\left(\boldsymbol{u}^e\right) = \int_{\Omega_e} \boldsymbol{B}^T \boldsymbol{\sigma} \mathrm{d}\Omega - \boldsymbol{P}^e = \mathbf{0} \tag{28}$$

where $\boldsymbol{P}^e$ is element nodal load. Substitute Eq. (22) into Eq. (28) and it is found that

$$\boldsymbol{K}^e\left(\boldsymbol{u}^e\right)\boldsymbol{u}^e = \boldsymbol{P}^e \tag{29}$$

where

$$\boldsymbol{K}^e = \boldsymbol{K}_L^e + \boldsymbol{K}_{NL}^e + \boldsymbol{K}_\sigma^e \tag{30}$$

denotes element secant stiffness matrix, in which

$$\boldsymbol{K}_L^e = \int_{\Omega_e} \boldsymbol{B}_L^T \overline{\boldsymbol{D}} \boldsymbol{B}_L \mathrm{d}\Omega \qquad \boldsymbol{K}_{NL}^e = \int_{\Omega_e} \boldsymbol{B}_L^T \overline{\boldsymbol{D}}\overline{\boldsymbol{B}}_{NL} \mathrm{d}\Omega \qquad \boldsymbol{K}_\sigma^e = \int_{\Omega_e} \boldsymbol{B}_{NL}^T \boldsymbol{\sigma} \mathrm{d}\Omega \tag{31}$$

where $\boldsymbol{K}_L^e$ is small displacement stiffness matrix with different moduli, $\boldsymbol{K}_{NL}^e$ is large displacement stiffness matrix with different moduli, and $\boldsymbol{K}_\sigma^e$ is initial stress stiffness matrix or geometric stiffness matrix with different moduli. Eq. (28) is the element total equilibrium equation and can be assembled and integrated into systematic equilibrium equation. From the element secant stiffness matrix above, it is found that the large deformation problem with different moduli is a double nonlinear problem including material nonlinear and geometric nonlinear factors.

With regard to the double nonlinear problem in this paper, for better tracing the loading balance path, judging and classifying critical point, the tangent stiffness matrix should be introduced. Therefore, in the following part, the tangent stiffness matrix with different moduli is deduced. The total derivative of Eq. (28) leads to

$$\mathrm{d}R\left(\boldsymbol{u}^e\right) = \int_{\Omega_e} \boldsymbol{B}^T \mathrm{d}\boldsymbol{\sigma} \mathrm{d}\Omega + \int_{\Omega_e} \mathrm{d}\boldsymbol{B}^T \boldsymbol{\sigma} \mathrm{d}\Omega \tag{32}$$

From Eq. (22), increment constitutive relation can be obtained as

$$d\boldsymbol{\sigma} = \overline{\boldsymbol{D}}_\tau d\varepsilon \tag{33}$$

Substitute Eq. (33) into the first term of the right side in Eq. (32) and get

$$\int_{\Omega_e} \boldsymbol{B}^T \mathrm{d}\boldsymbol{\sigma} \mathrm{d}\Omega = \int_{\Omega_e} \boldsymbol{B}^T \overline{\boldsymbol{D}}_\tau \mathrm{d}\boldsymbol{\varepsilon} \mathrm{d}\Omega = \int_{\Omega_e} \boldsymbol{B}^T \overline{\boldsymbol{D}}_\tau \boldsymbol{B} \mathrm{d}\Omega \mathrm{d}\boldsymbol{u}^e = \boldsymbol{K}_D^e \mathrm{d}\boldsymbol{u}^e \tag{34}$$

where $\boldsymbol{K}_D^e$ is tangent stiffness matrix. Substitute Eq. (25) into Eq. (34) and get

$$\boldsymbol{K}_D^e = \boldsymbol{K}_{DL}^e + \boldsymbol{K}_{DNL}^e \tag{35}$$

where

$$\boldsymbol{K}_{DL}^e = \int_{\Omega_e} \boldsymbol{B}_L^T \overline{\boldsymbol{D}}_\tau \boldsymbol{B}_L \mathrm{d}\Omega \quad \boldsymbol{K}_{DNL}^e = \int_{\Omega_e} \left(\boldsymbol{B}_L^T \overline{\boldsymbol{D}}_\tau \boldsymbol{B}_{NL} + \boldsymbol{B}_{NL}^T \overline{\boldsymbol{D}}_\tau \boldsymbol{B}_L + \boldsymbol{B}_{NL}^T \overline{\boldsymbol{D}}_\tau \boldsymbol{B}_{NL}\right) \mathrm{d}\Omega \tag{36}$$

where $\boldsymbol{K}_{DL}^e$ is small displacement stiffness matrix with different moduli, and $\boldsymbol{K}_{DNL}^e$ is large displacement stiffness matrix with different moduli. In addition, the second term for the right side of Eq. (32) can be expressed as

$$\int_{\Omega_e} \mathrm{d}\boldsymbol{B}^T \boldsymbol{\sigma} \mathrm{d}\Omega = \boldsymbol{K}_\sigma^e \mathrm{d}\boldsymbol{u}^e \tag{37}$$

where

$$\boldsymbol{K}_{\sigma}^{e}=\int_{\Omega_e}\boldsymbol{G}^{T}\hat{\boldsymbol{\sigma}}\boldsymbol{G}\mathrm{d}\Omega \tag{38}$$

where $\boldsymbol{K}_{\sigma}^{e}$ is initial matrix or geometric matrix. Substitute Eq. (35) and Eq. (38) into Eq. (32) and get

$$\mathrm{d}R\left(\boldsymbol{u}^{e}\right)=\boldsymbol{K}_{\tau}^{e}\mathrm{d}\boldsymbol{u}^{e} \tag{39}$$

where

$$\boldsymbol{K}_{\tau}^{e}=\boldsymbol{K}_{DL}^{e}+\boldsymbol{K}_{DNL}^{e}+\boldsymbol{K}_{\sigma}^{e} \tag{40}$$

where $\boldsymbol{K}_{\tau}^{e}$ is element tangent stiffness matrix with different moduli. It should be noted that $\hat{\boldsymbol{\sigma}}$ is symmetric matrix. If $\overline{\boldsymbol{D}}_{\tau}$ is also symmetric matrix, then so is $\boldsymbol{K}_{\tau}^{e}$. The $\boldsymbol{K}_{\tau}^{e}$ can be integrated into systematic tangent stiffness matrix $\boldsymbol{K}_{\tau}$. From the deduced tangent stiffness matrix above, it is also found that the large deformation problem with different moduli is a double nonlinear problem including material nonlinear and geometric nonlinear factors.

5.3 Finite element calculation using arc-length method

In this paper, arc length method (Crisfield 2000) is used to obtain buckling critical load of rod with different moduli. The total iterative formulation of calculation is as follows

$$\begin{cases}\lambda_{n}^{r}=\lambda_{n-1}+\Delta\lambda_{n}^{r}\\ K_{\tau}(\boldsymbol{u}_{n-1}+\Delta\boldsymbol{u}_{n}^{r-1})\Delta\boldsymbol{u}_{n}^{r}=\lambda_{n}^{r}\boldsymbol{P}\\ \boldsymbol{u}_{n}^{r}=\boldsymbol{u}_{n-1}+\Delta\boldsymbol{u}_{n}^{r}\end{cases} \tag{41}$$

where λ is parameter of proportional loading. Compared with the computation model with the same modulus, the constitutive relation of elastic theory with different moduli is relative to stress state, that is $\overline{\boldsymbol{D}}=\overline{\boldsymbol{D}}(\boldsymbol{\sigma})$. Therefore, small displacement stiffness matrix $\boldsymbol{K}_{DL}$, which $\boldsymbol{K}_{DL}=\boldsymbol{K}_{DL}(\boldsymbol{\sigma})=\boldsymbol{K}_{DL}(\boldsymbol{u})$, is not a constant anymore.

For large deformation finite element with different moduli, when compared with general finite element calculation process of geometric nonlinearity, principal stress state of each element should be judged in every iterative step in order to obtain corresponding elastic matrix. The increment equilibrium equation can be written as

$$K_{\tau}(\boldsymbol{u}_{n-1}+\Delta\boldsymbol{u}_{n}^{r-1})\Delta\boldsymbol{u}_{n}^{r}=(\boldsymbol{K}_{DL}(\boldsymbol{u}_{n-1}+\Delta\boldsymbol{u}_{n}^{r-1})+\boldsymbol{K}_{DNL}(\boldsymbol{u}_{n-1}+\Delta\boldsymbol{u}_{n}^{r-1})+\boldsymbol{K}_{\sigma}(\boldsymbol{u}_{n-1}+\Delta\boldsymbol{u}_{n}^{r-1}))\Delta\boldsymbol{u}_{n}^{r}=\lambda_{n}^{r}\boldsymbol{P} \tag{42}$$

In the calculation process of each increment step, firstly, by solving equilibrium equation $\left(\boldsymbol{K}_{DL}(\boldsymbol{u}_{n-1}+\Delta\boldsymbol{u}_{n}^{r-1})\right)\Delta\boldsymbol{u}_{n}^{r}=\lambda_{n}^{r}\boldsymbol{P}$, the initial increment displacement of small deformation mode is obtained. And then we solve equilibrium equation of large deformation finite element $\left(\boldsymbol{K}_{DL}(\boldsymbol{u}_{n-1}+\Delta\boldsymbol{u}_{n}^{r-1})+\boldsymbol{K}_{DNL}(\boldsymbol{u}_{n-1}+\Delta\boldsymbol{u}_{n}^{r-1})+\boldsymbol{K}_{\sigma}(\boldsymbol{u}_{n-1}+\Delta\boldsymbol{u}_{n}^{r-1})\right)\Delta\boldsymbol{u}_{n}^{r}=\lambda_{n}^{r}\boldsymbol{P}$. To make sure that interaction effect between material nonlinearity and geometric nonlinearity can be accurately considered, the constitutive relation with different moduli should be obtained through repeated iteration process during every step of geometric nonlinearity iteration.

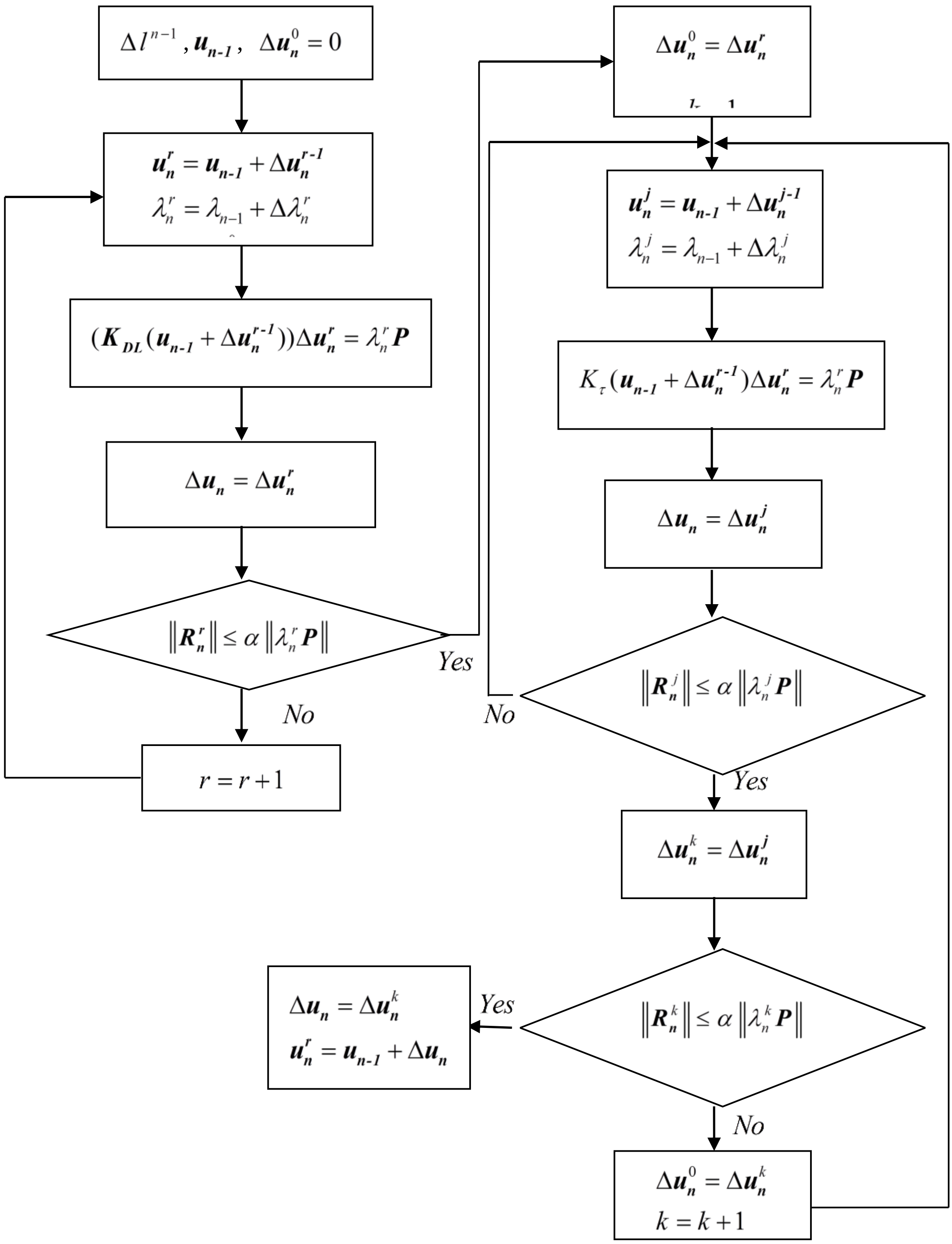

Fig. 4 Flowchart of large deformation finite element calculation with different moduli

The calculation process of the *n*-th loading increment step is portrayed in Fig. 4. In this figure, *r* denotes the iteration steps of equation $\left(\boldsymbol{K}_{DL}(\boldsymbol{u}_{n\text{-}1}+\Delta\boldsymbol{u}_n^{r\text{-}1})\right)\Delta\boldsymbol{u}_n^r=\lambda_n^r\boldsymbol{P}$, *j* and *k* represent material nonlinearity iteration steps and geometric nonlinearity iteration steps of equation $\left(\boldsymbol{K}_\tau(\boldsymbol{u}_{n\text{-}1}+\Delta\boldsymbol{u}_n^{r\text{-}1})\right)\Delta\boldsymbol{u}_n^r=\lambda_n^r\boldsymbol{P}$ respectively.

6. Test and model validation

For a validation of EM and FEM (EM and FEM are abbreviations for energy method and finite element method respectively), experiments were designed to perform tests on the mechanical properties of graphite (MSL82) specimens using an electronic universal testing machine (WDW-E100) and an electronic universal testing machine (CMT5306). The tests include the following: (1) uniaxial compressive test, (2) uniaxial tensile test and (3) buckling test.

6.1 Material mechanical properties tests

In the uniaxial tensile test, four specimens were made of graphite (MSL82). The size of the cylindrical specimens were radius=10 mm and height=50 mm. While in the uniaxial compressive test, the size of the four cylindrical specimens were radius=10 mm and height=200 mm. The results of these tests include the ultimate tensile strength, ultimate compressive strength, tensile elastic modulus, compressive elastic modulus and calculated E_c/E_t. The test results are tabulated in Table 1.

6.2 Buckling tests

The buckling tests are conducted in the electronic universal testing machine (WDW-E100) which is shown in Fig. 5(a). The configuration and dimensions (500mm×30mm×30mm) of graphite(MSL82) specimens are shown in Fig. 5(b) and Fig. 5(c). Test results are tabulated in Table 2 and plotted in Fig. 6(a). The results of energy method and finite element method are shown in Fig. 6(b).

Table 1 Test results on the mechanical properties of Graphite (MSL82)

Specimen number	Ultimate tensile strength (MPa)	Ultimate compressive strength (MPa)	Tensile elastic modulus (GPa)	Compressive elastic modulus (GPa)	E_c/E_t
1	8.389	22.858	8.62	11.90	1.38
2	9.646	21.480	8.59	12.32	1.43
3	9.038	20.426	8.84	12.58	1.42
4	8.389	22.291	8.73	12.26	1.40
Mean	8.866	21.764	8.70	12.27	1.41

Table 2 Buckling tests results, EM solutions, and FEM solutions

Specimen number	1	2	3	Mean	EM solutions	FEM solutions
Buckling critical load (kN)	34.58	25.38	34.78	31.58	32.53	32.09

(a)

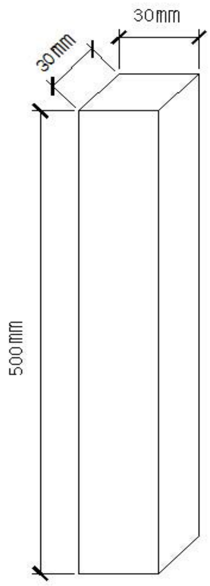

(b)

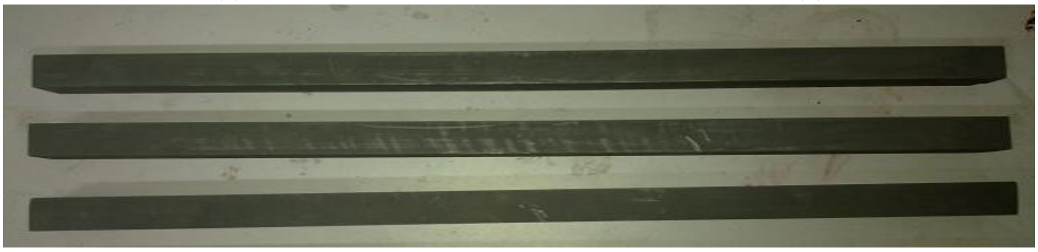

(c)

(d)

Fig. 5 (a) Testing device, (b) specimen size, (c) specimen of graphite materials (MSL82) before tests, and (d) specimen of graphite materials (MSL82) after tests

As depicted in Fig. 6(b), there is a good coincidence between EM solutions and the FEM solutions. However, EM solutions are larger probably because the assumed deflection curve actually may make stiffness of rod stronger, thus leading to relatively higher buckling critical load. The error of the two methods is within 5.5% and increases with growing displacement. Furthermore, by comparing EM and FEM solutions with the test results (see Fig. 6), for the graphite material (MSL82) with E_c/E_t of 1.41, there is a good agreement with a difference within 6.6%. Thus, EM and FEM developed in this paper are accurate and reliable.

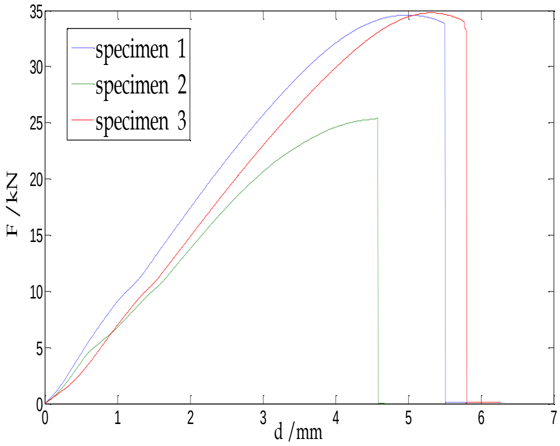

(a)

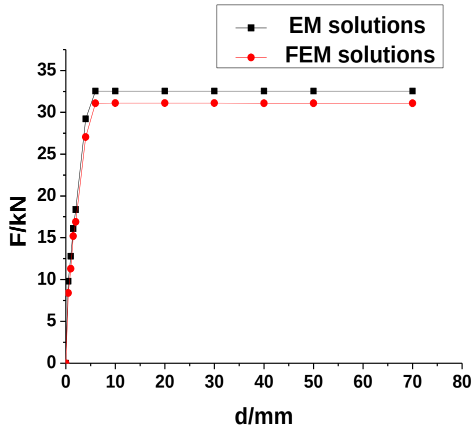

(b)

Fig. 6 (a) Relation of test load and axial displacement, and (b) relation of load and axial displacement for EM and FEM

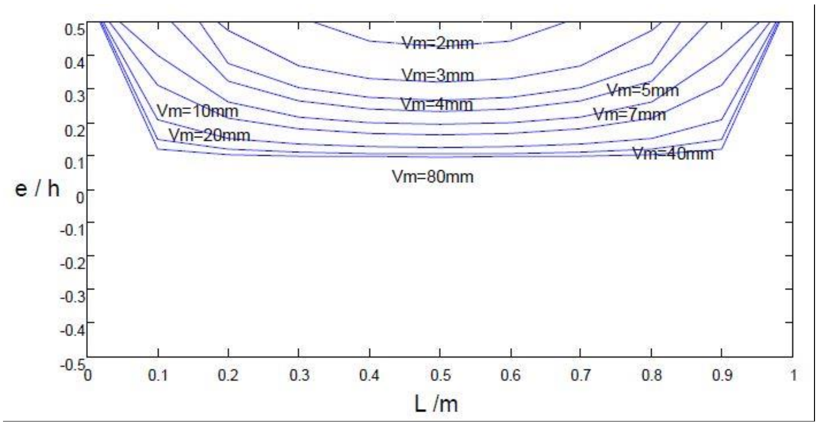

(a)

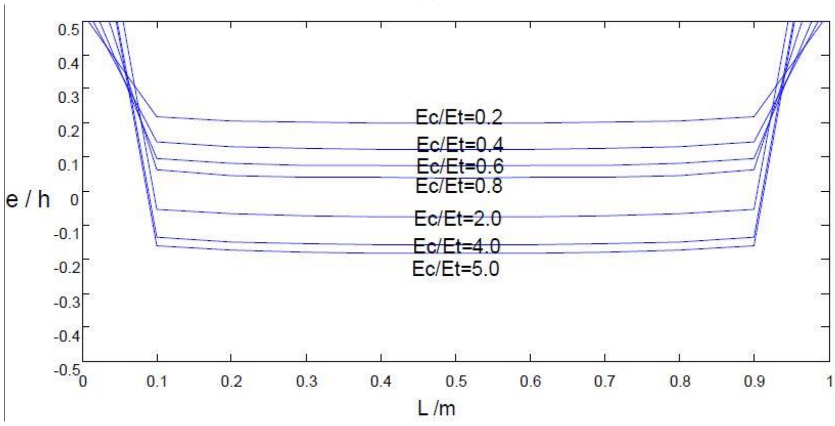

(b)

Fig. 7 (a) Variation of neutral axis with deflection (*m*=0.5), and (b) variation of neutral axial in the ultimate steady state with length of rod

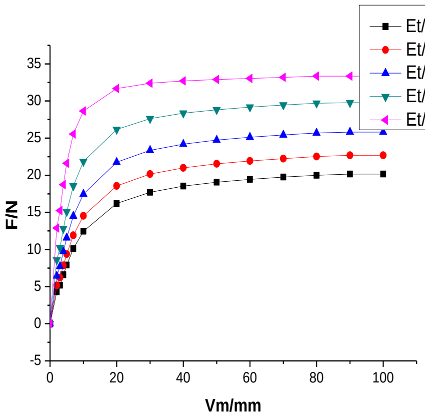

(a)

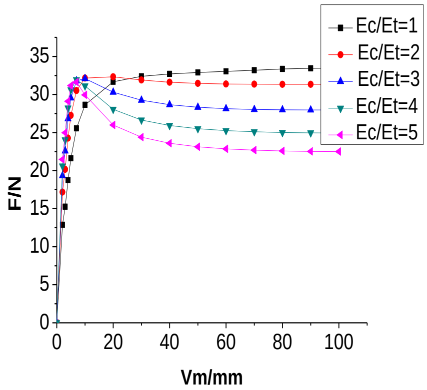

(b)

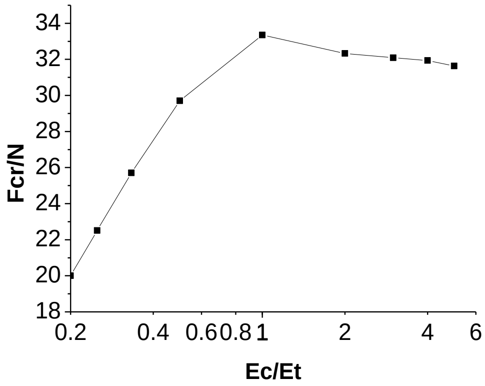

(c)

Fig. 8 Relation of load and deflection of rod when the average modulus E=4000MPa with (a) E_t/E_c=1.0~5.0, and (b) E_c/E_t=1.0~5.0; (c) Variation of buckling critical load against E_c/E_t

7. Example and discussion

7.1 Example

The EM and FEM are verified by tests in this paper. For further analyzing mechanical behavior of buckling rod with different moduli under experiencing large deformation, an example is given as follows. Consider a simply supported rod, as shown in Fig. 2(a), where the dimensions of this model are as follows: L=1 m, $b\times h$=0.01m×0.01m. An axial force F applied in the center at one end of the rod. A different elastic modulus is assumed for the following three cases: (1) $E=(E_c+E_t)/2$=4000 MPa, E_c/E_t and E_t/E_c=0.2~5; (2) E_t=1000 MPa, E_c/E_t=0.2~5; (3) E_c=1000 MPa, E_t/E_c=0.2~5. This example is solved by EM in this paper.

7.2 The difference between different moduli and same modulus problems

7.2.1 Neutral axis

When a different modulus is introduced, with the increase of V_m, regular variations occur in the neutral axis, as shown in Fig. 7(a). As deflection of rod approaches a certain value, the neutral axis reaches a stable equilibrium poison and will not move anymore, which is shown in Fig. 7(b). With the increase of *m*, the neutral axis gradually moves from the tensile zone to the compressive zone. In other words, the height of tension region tends to increase and vice versa.

7.2.2 Keeping the average modulus E=4000MPa unchanged

As shown in Fig. 8(a), when E_t/E_c is within the range of 1.0~5.0, with the increase of deflection, the load begins to rise linearly and rapidly, and then grows nonlinearly until a stable value. At this moment, the rod reaches buckling critical state, and with E_t/E_c increasing, buckling critical load of rod will decrease.

When E_c/E_t is within the range of 1.0~5.0, with deflection starting to increase slightly, the load develops linearly to the maximum value. For different E_c/E_t, the maximum loads are almost coincident. At the moment, the rod buckles and can not bear larger external load. Then with the continuous increase of deflection, the load declines nonlinearly and more quickly due to increasing of E_c/E_t until reaches a steady value (see Fig. 8(b))

The critical buckling load is smaller, whether E_c/E_t increases or decreases, than that of a rod with the same modulus. Moreover, the critical buckling load is more sensitive to the reduction of E_c (see Fig. 8(c) with the logarithmic coordinate for the transverse axis).

7.2.3 Keeping Et (or Ec)=1000MPa unchanged

As shown in Fig. 9(a-b), with E_t constant at 1000MPa, for different E_c/E_t, the variation of load against deflection are not so identical. When $E_c/E_t \leqslant 1.0$, with deflection increasing, the load initially develops rapidly and then nonlinearly grows till a stable value. The buckling critical load enhances with the increase of E_c. By contrast, when $E_c/E_t >1.0$, the load increases to the maximum value at the very start and then declines to a stable value. With the increase of E_c, the load develops more quickly together with the maximum value going up.

With one of the moduli remaining unchanged, increasing the other moduli leads to a differently regional increase of F_{cr}, as shown in Fig. 10(a). That is, F_{cr} shows a notable change from 2.75 kN to 8.20 kN (3 times the original value) when E_c increases by a factor of 5, from 200 MPa to 1000 MPa. It indicates that F_{cr} develops quickly and obviously. However, when E_c varies from 1000 MPa to 5000 MPa (increases by a factor of 5 as well), F_{cr} increases relatively slowly compared with the above results (only increases by a factor of 2.8). In addition, increasing E_t results in a more obvious and differently regional increase of F_{cr}. Compared with E_c, E_t has a less remarkable contribution to the enhancement of F_{cr}.

7.3 The difference between large deformation and small deformation problems

Comparing the results from small deformation problem with large deformation results calculated in this paper, as shown in Fig. 10(b), when E_c/E_t>1, the large deformation results are larger than those of small deformation problem. Moreover, with the increase of E_c/E_t, the errors enlarge and reaches the maximum 46.9% when E_c/E_t=5.

The maximum error between the calculated large deformation results and tests results, which is less than those of small deformation problem, is only 3% (see Table 2). It suggests that the results based on the large deformation theory are more close to reflect actual mechanical behavior and therefore, the EM model and FEM model proposed in this paper are feasible and accurate.

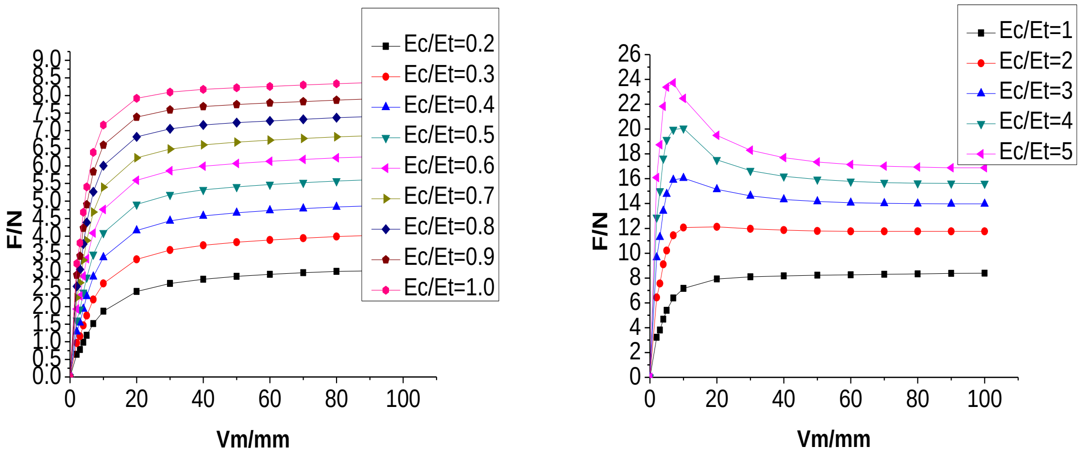

(a) (b)

Fig. 9 Relation of load and deflection of rod when Et =1000MPa with (a) E_c/E_t=0.2~1.0, and (b) E_c/E_t=1.0~5.0

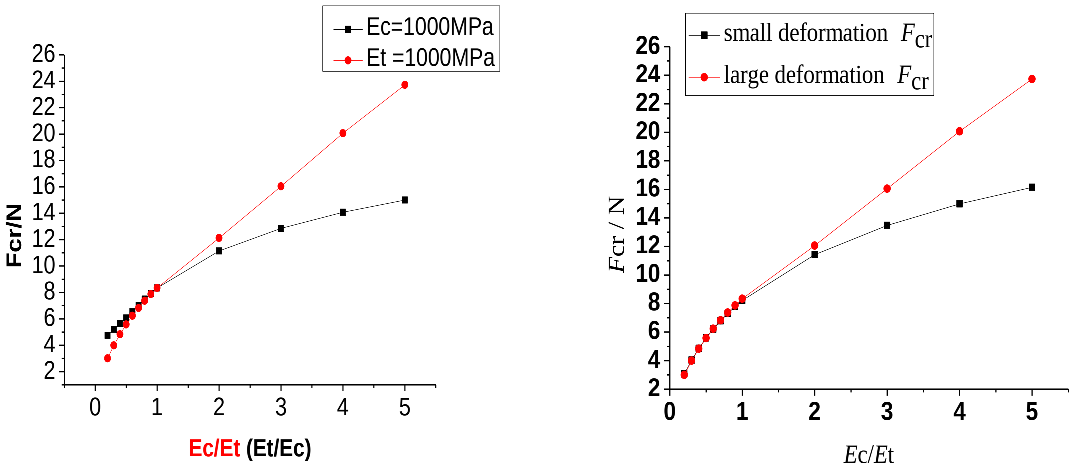

(a) (b)

Fig. 10 (a) Variation of buckling critical load against ratio of different moduli, and (b) comparison of results from large deformation and small deformation with different moduli (E_t=1000MPa)

8. Conclusions

In this paper, for analyzing the nonlinear buckling behavior of slender rod with different moduli under large deformation, the EM model and FEM model are established. The results of the proposed models are fairly identical. Meanwhile, the errors between the results of the proposed models and laboratory results are within 3%. Thus, the methods proposed in this paper are accurate and reliable. Based on this, effects of different moduli on nonlinear buckling of rod are investigated. Some conclusions are drawn as follows.

(1) When the average of the different moduli is constant, the buckling critical load decreases

with increasing difference between the different moduli because of the uneven distribution (discrete distribution) of stiffness within the section, which is caused by the difference of the different moduli. This uneven stiffness will induce a weakening effect on the resistance to buckling. Therefore, for graphene, the strongest material yet known, when it is applied into engineering, we should not only focus on graphene's ultimate strength, but also be aware of its relatively weak buckling resistance ability resulted from its property of different moduli. It is desirable to analyze the buckling behavior of structures composed of graphene by different moduli theory.

(2) When only one modulus increases while the other remains unchanged, the increase of the critical buckling load is regionally different. When E_c/E_t (E_t/E_c) $\leqslant 1$, the buckling critical load increases quickly, which indicates that, due to the increase of the modulus, the section stiffness increases and gradually becomes homogeneous, which accounts for a notable improvement in the ability of the rod to resist buckling. When E_c/E_t (E_t/E_c)>1, the critical load increases slowly because the gap of the modulus widens, which results in an uneven distribution of stiffness within the section. And the increase of E_c has a more remarkable effect on the enhancement of F_{cr} than that of E_t.

(3) Based on the large deformation theory, the calculated buckling critical load is larger than that based on small deformation theory. And the error between the results is growing with the increase of E_c/E_t, which indicates that, for this kind of material with different moduli, if the small deformation calculation method is still adopted, the deviation is too large. Thus, the calculation methods based on the large deformation theory can better authentically describe nonlinear mechanical behavior of structures with different moduli.

The EM model is simple and straightforward, low cost of computation, and effective. By contrast, the FEM model is relatively more accurate though time-consuming and slowly convergent. The models proposed in this paper could provide a novel and simple approach for further investigation of double non-linear mechanical behavior for structures composed of a material having different moduli.

Acknowledgements

Research supports from the National Natural Science Foundation of China (11072143, 11272200) are sincerely acknowledged by the authors.

References

Ambartsumyan, S. A. (1986), *Elasticity Theory of Different Modulus*, China Railway Press, Bei Jing, China.

Barak, M.M., Curry, J.D., Weiner, S. and Shahar, R. (2009), "Are tensile and compressive Young`s moduli of compact bone different", *J. Mech. Behav. Biomed. Mater.*, **2**, 51-60.

Bert, C.W. (1977), "Models for fibrous composites with different properties in tension and compression", *ASME J. Eng. Mater. Technol.*, **99**, 344-349.

Bert, C.W. and Ko, C.L. (1985), "Buckling of columns constructed of bimodular materials". *Int. J. Eng. Sci.*, **23** (6), 641-657.

Bruno, D., Lato, S. and Sacco, E. (1994), "Nonlinear analysis of bimodular composite plates under compression", *Comput. Mech.*, **14**, 28-37.

Crisfield, M.A. (2000), *Nonlinear Finite Element Analysis of Solids and Structures, Volume 1: Essentials,*

Crisfield Imperial College of Science, Technology and Medicine, London, UK.
Geim, A.K. (2009), “Graphene: status and prospects”, *Sci.*, **324**, 1530-1534.
Gilbert, G. (1961), “Stress/strain properties of cast iron and Poisson’s ratio in tension and compression”, *Brit. Cast Res. Assn. J.*, **9**, 347-363.
Gong, X.N., Wang, Q.T. and Luo, X. (1994), “Round hole expansion problem of bimodulus materials”, *J. Appl. Mech.*, **11**(4), 127-132.
Guo, Z.H. and Zhang, X.Q. (1987), “Investigation of complete Stree-deformation curves for concretes in tension”, *ACI Mater. J.*, **84** (4), 278-285.
Haimson, B.C. and Tharp, T.M. (1974), “Stresses around borehole in bilinear elastic rock”, *Soc. Petrol. Engrs. J.*, **14**, 145-151.
He, X.T., Chen, S.L. and Sun T.Y. (2007), “Applying the equivalent section method to solve beam subjected to lateral force and bend-compression column with different moduli”, *Int. J. Mech. Sci.*, **49**, 919-924.
He, X.T., Zheng, Z.L., Sun, J.Y., Li, Y.M. and Chen, S.L. (2009), “Convergence analysis of a finite element method based on different moduli in tension and compression”, *Int. J. Solid. Struct.*, **46** (20), 3734-3740.
Jones, R.M. (1977), “Stress-strain relations for materials with different moduli in tension and compression”, *J. AIAA*, **15**, 16-23.
Kratsh, K.M., Schutzler, J.C. and Eitman, D.S. (1972), “Carbon-carbon 3-D orthogonal material behavior”, *AIAA/ASME/SAE 13th Structures, Structural Dynamics and Material Conference*, San Antonio, Texas, USA, April.
Lan, T., Lin, P.D. and Chen, L.W. (2003), “Thermal buckling of bimodular sandwich beams”, *Compos. Struct.*, **25**, 345-352.
Leal, A. (2009), “Compressive strength analysis for high performance fibers with different modulus in tension and compression”, *J. Compos. Mater.*, **43**(6), 661-674.
Liu, X.B. and Zhang, Y.Z. (2000), “Modulus of elasticity in shear and accelerate convergence of different extension-compression elastic modulus finite element method”, *J. Dalian Univ. Tech.*, **40** (5), 526-530. (in Chinese)
Patel, B.P. (2004), “Thermo-flexural analysis of thick laminates of bimodulus composite materials”, *Compos. Struct.*, **63**(1), 11-20.
Patel, H.P., Turner, J.L. and Walter, J.D. (1976), “Radial tire cord-rubber composites”, *ASME Rub. Chem. Technol. Trans.*, **49**, 1095-1110.
Qu, C. (2009), “Deformation of geocell with different tensile and compressive modulus”, *J. Geotech. Geoenviron.*, **14**, 1-14.
Raffaele, Z. and Fabrizio, G. (2001), “Damage evolution in bimodular laminated composites under cyclic loading”, *Compos. Struct.*, **53**(4), 381-402.
Rigbi, Z. (1973), “The buckling of bimodular columns”, *Acta Mechanica*, **18**, 317-332.
Rizzi, E., Papa, E. and Corigliano, A. (2000), “Mechanical behavior of a syntactic foam: experiments and modeling”, *Int. J. Solid. Struct.*, **37**, 5773-5794.
Rigbi, Z. and Shmolo, I. (1978), “Buckling and immediate post buckling behavior of bimodular columns”, *J. Struct. Mech.*, **6**(2), 145-164.
Tseng, Y.P. and Jiang, Y.C. (1998), “Stress analysis of bimodular laminates using hybrid stress plate element”, *Int. J. Solid. Struct.*, **35**(17), 2025-2028.
Tsoukleri, G., Parthenios, J., Papagelis, K., Jalil, R., Ferrari, A., Geim, A., Novoselov, K. and Galiotis, C. (2009), “Subjecting a graphene monolayer to tension and compression”, *Small*, **5**, 2397-2402.
Vijayakumar, K. and Ashoka, J.G. (1990), “A bilinear constitutive model for isotropic bimodulus materials”, *ASME J. Eng. Mater. Technol.*, **112**, 372-379.
Yao, W.J. and Ye, Z. (2004), “Analytical solution of bending-compression column using different tension-compression modulus”, *Appl. Math. Mech.*, **25** (9), 901-909. (English Edition)
Yao, W.J. and Ye, Z. (2004), “Analytical solution for bending beam subject to later force with different modulus”, *Appl. Math. Mech.*, **25**(10), 1014-1022. (English Edition)
Yao, W.J. and Ye, Z. (2006), “Internal forces for statically indeterminate structures having different moduli in tension and compression”, *ASCE J. Eng. Mech.*, **132**(7), 739-746.

Yao, W.J., Zhang, C.H. and Jiang, X.F. (2006), "Nonlinear mechanical behavior of combined members with different moduli", *Int. J. Nonlin. Sci. Numer. Simul.*, **7**(2), 233-238.
Yang, H.T. and Wang, B. (2008), "An analysis of longitudinal vibration of bimodular rod via smoothing function approach", *J. Sound Vib.*, **317**, 419-431.
Yang, H.T., Wu, R.F. and Yang, K.J. (1992), "Solution to problem of dual extension-compression elastic modulus with initial stress method", *J. Dalian Univ. Tech.*, **32** (1), 35-39. (in Chinese)
Yang, H.T., Yang, K.J. and Wu, R.F. (1999), "Solution of 3-D elastic dual extension-compression modulus problems using initial stress technique", *J. Dalian Univ. Tech.*, **39** (4), 478-482. (in Chinese)
Yang, H.T. and Zhu, Y.L. (2006), "Solving elasticity problems with bi-modulus via a smoothing technique", *J. Comput, Mech.*, **23**(1), 19-23.
Ye, Z.M., Yu, H. and Yao, W.J. (2001), "A new elasticity and finite element formulation for different Young's modulus when tension and compression loading", *J. Shanghai Univ.*, **5** (2), 89-92. (in Chinese)
Zhang, Y.Z. and Wang, Z.F. (1989), "Algorithm for frames of bimodulus materials", *J. Dalian Univ. Tech.*, **29**(1), 23-32. (in Chinese)
Zhang, Y.Z. and Wang, Z.F. (1989), "Finite element method of elasticity problem with different tension and compression moduli", *Compu. Struct. Mech. Appl.*, **6** (1), 236-245. (in Chinese)

CC